Journal Pre-proof

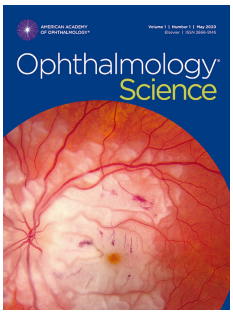

Individualized Estimation of Baseline Retinal Nerve Fiber Layer Thickness Using Conditional Variational Autoencoder

Ou Tan, Keke Liu, Aiyin Chen, Dongseok Choi, Jonathan C.H. Chan, Bonnie N.K. Choy, Kendrick C. Shih, Jasper K.W. Wong, Alex L.K. Ng, Janice J.C. Cheung, Michael Y. Ni, Jimmy S.M. Lai, Gabriel M. Leung, Ian Y.H. Wong, David Huang

PII: S2666-9145(25)00147-2

DOI: https://doi.org/10.1016/j.xops.2025.100849

Reference: XOPS 100849

To appear in: *Ophthalmology Science*

Received Date: 28 March 2024

Revised Date: 30 May 2025

Accepted Date: 2 June 2025

Please cite this article as: Tan O., Liu K., Chen A., Choi D., Chan J.C.H., Choy B.N.K., Shih K.C., Wong J.K.W., Ng A.L.K., Cheung J.J.C., Ni M.Y., Lai J.S.M., Leung G.M., Wong I.Y.H. & Huang D., Individualized Estimation of Baseline Retinal Nerve Fiber Layer Thickness Using Conditional Variational Autoencoder, *Ophthalmology Science* (2025), doi: https://doi.org/10.1016/j.xops.2025.100849.

Individualized Estimation of Baseline Retinal Nerve Fiber Layer Thickness Using Conditional Variational Autoencoder

Running head: Individualized baseline NFL thickness

Journal: Ophthalmology Science

Author: Ou Tan[1], Keke Liu[1,2] , Aiyin Chen[1], Dongseok Choi[1], Jonathan C.H. Chan[3], Bonnie N.K. Choy[3], Kendrick C. Shih[3], Jasper K.W. Wong[3], Alex L.K. Ng[3], Janice J.C. Cheung[3], Michael Y. Ni[4,5,6], Jimmy S.M. Lai[3], Gabriel M. Leung[4], Ian Y.H. Wong[3,7], David Huang[1]

1Casey Eye Institute, Oregon Health & Science University, Portland, Oregon, USA

2Department of Ophthalmology, Duke University School of Medicine, Durham, North Carolina, USA

3Department of Ophthalmology, LKS Faculty of Medicine, The University of Hong Kong, The University of Hong Kong, Hong Kong

4School of Public Health, LKS Faculty of Medicine, The University of Hong Kong, Hong Kong Special Administrative Region, China

5The State Key Laboratory of Brain and Cognitive Sciences. The University of Hong Kong, Hong Kong Special Administrative Region, China

6Healthy High Density Cities Lab, HKUrbanLab, The University of Hong Kong, Hong Kong Special Administrative Region, China

7Department of Ophthalmology, Hong Kong Sanatorium & Hospital, Hong Kong.

Corresponding Author: David Huang, MD, PhD

David Huang, MD, PhD

Casey Eye Institute

Oregon Health & Science University

515 SW Campus Drive, CEI 3154, Portland, OR 97239

Phone: (503) 494-0633

huangd@ohsu.edu

Financial Support: Financial Support: This study was supported by NIH grants R01 EY023285, R21 EY032146, P30 EY010572, the Malcolm M Marquis, MD Endowed Fund for Innovation and an unrestricted grant from Research to Prevent Blindness to Casey Eye Institute. The sponsor or funding organization had no role in the design or conduct of this research.

Conflict of interest statement: OHSU, Dr. Tan, Dr. Huang have a significant financial interest in Visionix, Inc., a company that may have a commercial interest in the results of this research and technology. These potential conflicts of interest have been reviewed and managed by OHSU.

Abbreviation list

AL	Axial Length
CVAE	Conditional variational autoencoder
rCNN	Convolutional neural network for regression
ILM	Inner limiting membrane
MLR	Multiple linear regression
OCT	Optical coherence tomography
RPE	Retina pigment epithelium
NFLT	Retinal nerve fiber layer thickness
SSI	Signal strength index
SE	Spherical equivalent refractive error

Key word: glaucoma, optical coherence tomography, nerve fiber layer thickness, conditional variational autoencoder

Abstract

Purpose: Use generative deep learning (DL) models to estimate baseline reference nerve fiber layer thickness (NFLT) profile, taking into account individual ocular characteristics.

Design: Cross-sectional study.

Participants: 686 individuals from the Hong Kong Family cohort and 75 individuals from the Casey Eye Institute (CEI) cohort.

Methods: Healthy eyes were selected from the Hong Kong FAMILY and CEI cohorts. Circumpapillary NFLT profiles and vascular patterns were measured by a spectral-domain optical coherence tomography (OCT). Generative DL models were trained using the FAMILY data to reconstruct the individualized baseline NFLT, a customized normal reference based on each eye's own vascular pattern, axial length (AL), spherical equivalent (SE) refractive error, disc size, and demography information. Two deep learning models were developed. The MAG model used actual AL and SE, while the REG model estimated AL and SE using vascular patterns as input. For comparison, a multiple linear regression (MLR) was trained to estimate baseline NFLT using AL and demographic information. Five-fold Cross-validation was used to assess performance.

Main Outcome Measures: The prediction error: root-mean-square of the difference between the actual NFLT profile and the predicted individualized baseline.

Results: A total of 1152 healthy eyes from 686 participants in the Hong Kong Family cohort were divided into four subgroups: high myopia (SE<-6D), low myopia (SE=-6D~-1D), emmetropia (SE=-1D~1D), and hyperopia (SE>1D). Compared with the population means, both DL models significantly reduced the prediction error for overall and quadrant NFLT and decreased the false-positive rate of identifying abnormal NFLT thinning in both myopia groups (from 13.0%-27.0% to 6.7%~9.4%). Both DL models significantly reduced prediction error for the NFLT profiles compared to both the population mean and the MLR-adjusted NFLT. The reductions in prediction errors for NFLT profile and overall NFLT value were independently validated using the CEI data.

Conclusions: Generative DL models (a type of artificial intelligence) can construct individualized NFLT baseline profiles using the vascular pattern derived from the same OCT scans. The individualized baseline reduced the prediction error of the NFLT profile in healthy eyes and may improve the accuracy of identifying abnormal NFLT thinning, especially in myopic eyes.

1 Introduction

Glaucoma is associated with the progressive loss of retinal nerve fiber layer thickness (NFLT).[1-3] Optical coherence tomography (OCT) is commonly used to detect and monitor nerve fiber layer thinning.[4, 5] Detection of pathological thinning is based on the premise that the NFLT measured in an individual person can be compared to a theoretical baseline value prior to disease onset. In conventional practice (i.e. the glaucoma diagnostic packages offered by OCT manufacturers) NFLT distribution in a healthy population is usually used as a generic baseline. Usually, a normative database with hundreds of healthy eyes would be collected for a specific OCT model in the Food & Drug Administration (FDA) clearance process. NFLT variation associated with demographic (age, race, sex) factors is accounted for by regression or matching with the patient to be tested. However, the conventional approach neglects significant variations in the NFLT associated with the vascular pattern and transverse optical magnification of the individual eye. Neglecting these individual variations can lead to false-positive diagnoses or false-negative misdiagnoses of glaucoma and other optic neuropathies.

A well-known problem of the conventional approach is the false positive diagnosis of glaucoma in highly myopic eyes, which have thinner measured NFLT globally (and in most sectors) due to higher axial length and lower transverse optical magnification. [6-11] The lower magnification causes the OCT scan pattern to span a larger area around the optic nerve head (ONH), and it is well known that the NFLT decreases with greater distance from the ONH in a roughly reciprocal fashion.[8]This problem is so common that it has earned the name “red disease” because values below the 1 percentile cutoff of the healthy population are typically printed in red on OCT displays. [12]

It is also known that the thickness peaks in the NFLT profile are at the superior and inferior arcuate bundles that generally collocate with the major arcade vessels.[13] Thus, the peripapillary vascular pattern measured on the OCT can be used to predict the NFLT peak location. The vascular pattern also contains information on the papillomacular axis, which is also known to influence the NFLT pattern. [14-18] Disc size is another measurable individual characteristic that is known to influence NFLT.[8, 19]

We define the individualized baseline as the customized normal reference that accounts for individual eye characteristics such as the vascular pattern and the transverse optical magnification, which can be represented by its determinants: the axial length (AL) and spherical equivalent (SE) refractive error. We hypothesize that an individualized baseline NFLT profile can serve as a better reference for detecting pathological thinning associated with glaucoma and other optic neuropathies. We further hypothesize that it is feasible to obtain an individualized baseline using the map of major retinal blood vessels that can be extracted from the same OCT scan used to produce the NFLT map, plus AL, SE, and demographic information. To generate the individualized baseline, we chose a deep learning generative model, a conditional variational autoencoder (CVAE). [20-23]

Recent studies have successfully used deep learning models to predict clinical features, such as gender, race, and AL.[20, 24-28] This encourages us to use deep learning to analyze the vascular pattern to generate information on AL and SE. We chose to use a convolutional neural network for regression analysis (rCNN)[29] to estimate individual features, such as AL and SE.

We developed three deep learning models, based on how the AL/SE was used: No AL/SE; measured AL/SE; AL/SE estimated by a rCNN. We compare their performance to a regression model. The performances for these various baseline references are compared by the prediction error, the root-

mean-square of the difference between the true NFLT parameters and the generated baselines. We also calculated the false positive rate (FPR) of detecting significant NFLT loss, stratified by myopic refractive error, to assess the effectiveness of reducing the "red disease" problem. The difference between the reference NFLT with the 5 percentile cutoffs is used as a preliminary estimation of potential gain in glaucoma diagnostic sensitivity.

2 Methods

2.1 Participants

2.1.1 Hong Kong Dataset

This cross-sectional study included participants from the Hong Kong FAMILY Cohort, a large territory-wide random sample of occupants from several Hong Kong districts. The Institutional Review Board of the University of Hong Kong approved the study, which adhered to the Declaration of Helsinki. Comprehensive details of the recruitment process and cohort characteristics were previously reported.[30] In brief, all participants older than 18 were invited to participate and provided consent prior to enrollment. All participants received a comprehensive ophthalmic examination, including visual acuity, subjective refraction, perimetry, keratometry, pachymetry, axial eye length, intraocular pressure, slit-lamp examination, and indirect ophthalmoscopy.[31] The axial eye length was measured with an ocular biometer (AL-Scan, Nidek, Gamagori, Japan).

Only healthy eyes were included in this study, and either one or two eyes were included per participant. The exclusion criteria were the following: subjects with a history of glaucoma, abnormal test in frequency doubling technology (FDT) perimetry or fundus examination (disc, macula, or vessels), elevated intraocular pressure (> 21 mm Hg), enlarged cup-to-disc ratio (> 0.7), pseudophakia, or missing data.

2.1.2 Casey Eye Institute Dataset

This case-control study was performed at the Casey Eye Institute (CEI), Oregon Health & Science University. The research protocol was approved by the institutional review board at Oregon Health & Science University and adhered to the tenets of the Declaration of Helsinki. Written informed consent was obtained from each participant.

Participants were part of the "Functional and Structural Optical Coherence Tomography for Glaucoma" study.[32] The inclusion criteria for normal control were (1) no history of glaucoma, retinal pathology, or current corticosteroid use; (2) no history of ocular hypertension as defined by IOP ≥ 22 mmHg; (3) normal Humphery 24-2 VF test; (4) normal optic nerve head and NFL appearance on funduscopy; (5) symmetric optic nerve head appearance between both eyes; (6) central pachymetry > 470 µm. The exclusion criteria were (1) best-corrected visual acuity less than 20/40; (2) previous intraocular surgery except for uncomplicated cataract extraction with posterior chamber intraocular lens implantation; (4) any diseases that may cause VF loss or optic disc abnormalities; (5) narrow anterior chamber angle by gonioscopy. Only one eye of each participant received OCT scanning and analysis. This CEI dataset was introduced to obtain independent validation of models trained on the Hong Kong dataset.

2.2 OCT Measurements

The NFLT and disc size were obtained from an optic nerve head (ONH) scan using a commercially available spectral-domain OCT device (Avanti with AngioVue OCTA, Visionix/Optovue Inc, Fremont, California, USA). The ONH scan contains 13 rings covering a 4.9 mm peripapillary area around the optic disc (Figure 1A). Raw OCT images, boundary segmentation, signal strength defined by the signal strength index (SSI, 0-100), disc size defined by disc area in mm^2, and the NFLT profile at diameter D=3.4mm were exported for data analysis in this study. An automated quality check algorithm was applied to OCT images to remove scans with poor SSI (SSI<35), retina cropping, or extremely low NFLT (NFLT value lower than 4 times the population Standard deviation in healthy eyes). Our previous study showed that SSI and disc size were also predictive factors of NFLT.[19, 33]

The vessel location was detected using the shadow of large vessels in the inner retina on the retinal pigment epithelium (RPE) (Figure 1B). An *en face* map of vessel intensity in the RPE complex was reconstructed from the vessel shadow profile on the 13 rings of the ONH scan. Then we applied a level-set method[34] to detect large vessels (Figure 1C).

The vascular pattern, NFLT, and boundary elevation profiles on different circles around the disc center were resampled from maps. Primarily, the NFLT profile and the vascular pattern profile at diameter=3.4mm were used as input for the generative deep learning model. The inner limiting membrane (ILM) and RPE elevation maps were also reconstructed, similar to the NFLT map.

2.3 Generative Deep Learning Models

A conditional variational convolutional autoencoder (CVAE) was used to encode and generate the NFLT profile. A second CVAE was used to encode and reconstruct the vascular pattern. The generation of NFLT by the first CVAE was conditioned on the encoded vascular pattern from the second CVAE. Both CVAEs were conditioned by factors associated with an individual person, eye, and scan: age, sex, AL, SE, disc size, and scan signal strength. We picked the variational autoencoder (VAE) architecture to address the issue of non-regularized latent space in the autoencoder and provide generative capability to the entire space. VAEs blend deep learning with probabilistic reasoning. Like an autoencoder, they have an encoder and decoder, but instead of just copying data, they learn the underlying probability distribution. This involves approximating the true distribution and minimizing the difference between them using a simpler one.[35] CVAE is a special type of VAE that adds individual factors to control the NFLT generation.[21] Most importantly, we connected two CVAEs by using the hidden space of the CVAE of the vascular pattern as a conditional input of the NFLT CVAE. The latent space of the vascular pattern CVAE provided vectors corresponding to an individual vascular pattern. Those vectors made the generated NFLT profile match the specific vascular pattern.

We designed three models, depending on how to use magnification factors. The details are included in the next sections.

2.3.1 Models in the Training Stage

We first proposed a BASE model, which has two parallel CVAEs (Figure 2A). Each CVAE had three parts: encode, decoder, and sampling block. In the encoder, firstly, we used a convolutional neural network (CNN) with several convolution blocks to convert profiles from one dimension in space into vectors in a higher dimension and reduce the transverse size to 1. Then, we used a concatenate layer that combined the output of CNN with conditions. A fully connected network converted the

concatenated vector into vectors representing the μ and σ in the latent space. The sampling blocks created random variables z~ N(μ, σ). In the decoder, the random variables were concatenated with conditions again. Then, a fully connected network, followed by several transverse Convolution blocks, reconstructed the profile. Conditions were different between the two CVAEs. The vascular pattern CVAE used demographic information, such as age and gender, as a condition. The NFLT CVAE used the demography information, plus the output from the vascular pattern CVAE, as the conditions. In the NFLT encoder, the output of the CNN of the vascular pattern CVAE was used as a condition for the vascular pattern. In the NFLT decoder, the output of the sample layer of the vascular pattern CVAE was used as a condition for the vascular pattern.

We then proposed a MAG model (Figure 2B). The structure was identical to the BASE model, except the conditions were updated to include magnification-related information, such as AL, SE, and disc area, SSI, besides the demographic information.

As AL and SE may not be available in commercial OCT, we also proposed a REG model, which used a predicted AL and SE based on OCT data. The magnification information had been estimated from the vascular pattern using disc photography in the literature.[27, 36, 37] We used a CNN for regression (rCNN) to predict the AL and SE using information from OCT and demographic information (Figure 2C). The rCNN includes convolution blocks and fully connected networks. The input of rCNN included the vascular pattern map (Figure 1C) and the RPE elevation map. We did not use the ILM elevation map because glaucoma would change the characteristics of the ILM surface.[38] Due to the limitation of the scan pattern, we used the available maps around the disc center (diameter=2~4mm). The rCNN was trained using the actual AL and SE data. Once trained, the AL and SE outputs of the rCNN were used to condition the CVAEs in the MAG model.

2.3.2 Loss Functions

The training is based on the minimization of the loss function. The loss function of a CVAE is a summation of reconstruction loss and regularization loss. The reconstruction loss included the mean square error (MSE, for continuous variables) or binary cross entropy (BCE, for binary variables) between the input and the estimated profile, while the regularization loss included Kullback-Leibler divergence (KL) between the distributions represented by the latent vector and a standard Gaussian distribution. The loss function of the rCNN is a summation of MSE of all outputs. Therefore, the loss function of the REG model was the summation of the loss functions of 2 CVAES and 1 rCNN.

$$Loss = MSE_{NFLT} + BCE_{VP} + KL_{VP} + KL_{NFL} + MSE_{AL} + MSE_{SE}$$

Here, NFLT was for CVAE for the NFLT profile, VP was for CVAE for the vascular pattern profile, and AL and SE were for the rCNN.

The loss function of the BASE and Mag models is similar to the above formula, but removes the last two MSE terms corresponding to the loss function of rCNN.

$$Loss = MSE_{NFLT} + BCE_{VP} + KL_{VP} + KL_{NFL}$$

2.3.3 Models in the Generating Stage

In the generating stage, only the vascular pattern CVAE encoder and the NFLT CVAE decoder were used (Figure 3A-C). To generate the baseline NFLT value of the individual eyes, we set the input of the NFL-CVAE decoder (Z1) to 0. If we sampled the Z1 from N(0, 1), which allowed the generalization of a group

of random vectors. If we combined them with a set of conditions, the NFLT decoder would generate a group of NFL thickness profiles corresponding to the same set of conditions. The variation in NFL thickness profiles will not be due to glaucoma damage, as the module is only trained on healthy eyes. We then might average them to get a normal reference for this given condition set. However, the average can also be approximated by using $\mu 1 = 0$ and $\sigma 1 = 0$, which only needs to run the module once, therefore significantly reducing the calculation cost. So, we forced Z1=0 to generate the normal reference.

Similarly, we use the output $\mu 2$ vector from the vascular pattern encoder directly as Z2, indicating the vascular pattern part in the NFLT decoder's conditions. Note that μ was calculated, different from 0, and represented the specific vascular pattern. Using the above two simplifications, we generate a normal reference matching the individual vascular pattern and other conditions.

In the generating stage, the BASE model included demographic information and the μ vector form vascular pattern encoder; the MAG model included all conditions in the BASE model plus AL, SE, and disc area; the REG model used similar conditions as the MAG model but replaced the AL and SE by the predicted value from the rCNN.

2.3.4 Normalization of Input

Glaucoma causes attenuation of retinal vascular caliber, which may affect the generation of individualized NFLT baseline reference and reduce the sensitivity of detecting disease. To avoid this potential pitfall, we normalized the vessel size of all eyes. The idea was to resize each vessel proportionally and keep a constant ratio of pixel numbers between vessels and non-vessels.

We normalized all inputs according to their mean and standard deviation to reduce the scale difference among features. The normalization accelerated and stabilized the learning process and avoided the problem of exploding gradients in the regression network.[39]

When both the left and right eyes were used for the same participant, the learning weight of each eye was halved in the training stage to equalize each participant's weight.

2.3.5 Training Algorithm and Parameter

In the training, we chose the Adam optimization algorithm (decay=0.001) to update network parameters. Dropout (0.5) and L2 (0.02) regularization were used to reduce overfitting. The initial learning rate was set to 0.001.

2.4 Multiple linear regression

The normative reference for NFLT can be improved by accounting for the effect of demographics, scan quality, and magnification. To assess the performance of this approach, we used multiple linear regression (MLR) with a mixed-effect model. Based on previous studies,[19] we identified age, sex, and SSI and AL as the optimal combination of independent variables in the model. A broken stick (or segmented) regression model related NFLT to AL. With the breakpoints set at emmetropia (SE = 0 diopters), the broken stick model divided healthy eyes into two segments: the hyperopia segment (SE>0) and the myopia segment (SE<0). The MLR was estimated for the overall average, sectoral averages, and each point on the NFL profiles. The normal reference is constructed by averaging all eyes after adjusting NFLT to a reference age/sex/SSI/AL based on the MLR. When we computed the prediction error or checked the abnormality of a testing eye, the NFLT was adjusted using the same scheme.

2.5 Statistical Analysis

In total, five models of normal reference were compared in this study: 1) population average without any adjustment(Average); 2) adjusted based on the multiple linear regression (MLR); 3) generated by the deep learning model without magnification information (BASE); 4) generated by deep learning model with magnification information, using true AL and SE directly (MAG); 5) generated by the deep learning model with AL and SE predictand by rCNN, (REG).

Based on the Hong Kong dataset, five-fold cross-validation was used to test the performance of the fully trained models. For each fold, we used 80% of the eyes to train the deep learning/MLR models and the remaining 20% of the eyes to test the performance of the trained model. The final performance was pooled from all folds. In the training of deep learning models, 10% of the training set was reserved for internal validation (not to be confused with the five-fold validation) to avoid overfitting.

The prediction error was estimated as the root-mean-square of the difference between the true value and the predicted value using a mixed-effect model. The false positive rates (FPR) were compared among models, using a generalized linear mixed-effect model (GLMM) equivalent to the McNemar test.[40] All analyses were done in MATLAB R2021b with the Statistics Toolbox and deep learning toolbox. Mixed-effect models were used to address between-eye correlation when applicable.

The models trained on the Hong Kong dataset were also applied to the CEI dataset. The prediction errors between the predicted normal reference and the tested eyes were estimated for the overall, quadrant, and profiles of NFL thickness. To compensate for the difference in NFL thickness due to race in two datasets, mainly East Asians in the Hong Kong dataset and multiple races in the CEI dataset, we proportionally adjusted the individualized baseline according to the ratio of the population average of NFL thickness profile between the emmetropia eyes in the two datasets. [41-45] To compare the prediction error among models, a mixed-effect model was fitted to each data set, followed by Dunnett's (post-hoc) test.

3 Results

3.1 Characteristics of the Study Participants

A total of 1152 healthy eyes from 686 participants with valid age, gender, AL, SE, and NFLT profiles were selected from the Hong Kong dataset (**Table 1**). Eyes were divided into four subgroups: 106 high myopia (SE<- -6 D), 509 low myopia (-6 to -1 D), 401 emmetropia (-1 D to 1 D), and 136 hyperopia (> 1 D). As expected, myopic eyes had longer AL, smaller disc size, and thinner NFL. Myopic eyes were also younger.

A total of 75 normal eyes from 75 participants were selected from the CEI dataset (last column, Table 1). The CEI dataset is relatively older and has fewer female participants than the Hong Kong dataset. A wide range of myopia eyes were included in the CEI dataset (SE=-14.5~5 D, AL=21.7~29.0 mm), but the average SE, AL, and Disc size of the CEI dataset were between emmetropia and low myopia in the Hong Kong dataset.

3.2 Training of Regression and Deep Learning Models

Based on the Hong Kong dataset, the association of NFLT with predictive factors varied between quadrants (**Table 2**). In the MLR with a broken stick model, NFLT was significantly associated with AL

(p<0.001) for overall average and superior, nasal, and inferior quadrants. Significant associations were also found for age and gender, with different quadrant distributions. Those slopes based on the MLR were used to adjust the NFLT in later analyses.

In the REG model, the correlation coefficient between the predicted value and the ground truth is 0.59±0.05 (p<0.001) for AL and 0.54±0.05 (p<0.001) for SE, based on 5-fold cross-validation. The correlation is moderate and much smaller than the correlation in the training, which was usually above 0.70. This indicated overfitting in the regression model. Experiments by choosing a larger dropout rate, larger L2, or shallower network reduced the overfitting in the training, but the correlation in the test dataset was in the same range.

The estimation of binary cross-entropy Loss of the vascular pattern of three deep learning models was similar (0.372~0.375). The MAG and REG models had smaller root mean square errors of NFL thickness prediction (8.27 and 8.20μm) than the BASE model (8.95μm).

3.3 Prediction Error between Actual NFLT and the Predicted Baseline Reference

A smaller NFLT prediction error in healthy eyes means that a tighter diagnostic threshold can be used at a given specificity level. This helps to detect glaucoma at an earlier stage when NFLT thinning is more subtle. We calculated the difference between the actual individual NFLT values and the predicted baseline reference for each of the 5 models. Then we compared the prediction error of the more advanced models to the simplest model (unadjusted population average), for which the prediction error was simply the population standard deviation in the test dataset.

Based on the Hong Kong dataset, the MAG and REG models had the smallest prediction error for the overall and quadrants (**Table 3**). They were significantly lower than the normal reference based on the population average. However, they were only significantly better than the MLR model in nasal (p<=0.01), but borderline for others (p<0.10). The BASE model did not significantly reduce the prediction error compared to the population average without adjustment.

Based on the Hong Kong Dataset, the original (population average) model had large prediction errors near the two prominent NFLT peaks (**Figure 4A**). This was expected as the location of these peaks (arcuate bundles) is known to vary between individuals. Compared to the original and MLR models, both the MAG and REG models greatly reduced the prediction error of the NFLT profile near the arcuate bundles. The BASE model also reduced the prediction error to a small degree. The MLR model did not significantly reduce the prediction error of NFLT at the arcuate bundles. This was expected as the inputs to the MLR model did not contain information on the location of the arcuate bundles.

Similar trends were observed based on the CEI dataset (**Table 3 and Figure 4B**). All models showed lower prediction error for overall and quadrants than the population average. The MAG models had the smallest prediction error among other models, except the inferior quadrant. (**Table 3**) For the Profile, the MAG deep learning model showed the smallest prediction errors in the superior quadrant and inferior-temporal sectors. All three deep learning models showed significantly smaller prediction error compared to both MLR and average models (root mean squares = 16.7 μm, 16.0μm, and 16.6μm vs. 18.7μm and 18.8μm, p<0.001). The prediction errors from the CEI dataset were larger than those from the Hong Kong dataset for all parameters and all models, including the population average. This indicates a greater variability in the CEI dataset, possibly because it is multiracial. We did not analyze the

effect of refractive error on the rate of false-positive abnormality in the CEI dataset because of the lack of highly myopic eyes.

3.4 False Positive Rate

False positive rates (FPR) were based on eyes with thickness below the 5th percentile cutoff of the normal reference. The cutoff was estimated from the histogram of the original NFLT or the adjusted NFLT in the emmetropia group. The REG model significantly reduced the FPR in the myopia and high myopia groups compared to the original value, except in the temporal area (**Table 4**). The REG model had a similar performance on FPR compared to MLR or MAG model in most of the parameters($p>0.05$). However, the MLR and MAG models showed more consistent FPR in all groups. In hyperopia, all models had similar FPR ($p>0.05$). For the temporal quadrant average of NFLT, the original value showed FPR significantly less than 5% in myopia groups, which might be due to the temporal NFL being less affected by magnification and the population variance in myopia groups being significantly lower than the emmetropia group.

3.5 Difference Between Normal Reference and Five Percentile Cutoff

Due to the lack of verified glaucoma eyes in the Hong Kong dataset, we cannot evaluate the diagnostic sensitivity directly. Instead, we estimated the difference between each model's normal reference/baseline and the 5-percentile cut-point. A tighter (smaller) difference indicated that glaucomatous eyes at earlier stages with smaller loss of NFLT could be detected. For a population of glaucomatous eyes that includes those with early disease, the ability to detect smaller deviations from the healthy baseline would lead to better diagnostic sensitivity. MLR and all deep learning models reduced the difference between the median and the 5-percentile cutoff, compared to the population average (**Table 5**). Among four adjusting models, two deep learning models with magnification information had smaller differences than other models, and the BASE model had the worst performance, though those comparisons are not statistically significant($p>0.0125$).

4 Discussion

In this study, we proposed deep learning models to estimate the individualized baseline NFLT profile. By taking into account individual variations in the transverse optical magnification (related axial eye length and refractive error) and anatomy (related to retinal vascular pattern), we hypothesize that the individualized baseline would help distinguish real pathology from normal inter-individual variation and serve as a more reliable diagnostic reference than the simple population-average NFLT profile and sector averages. Our models are based on CVAE, which estimates the individualized baseline NFLT profile using the vascular pattern profile derived from the OCT scan, as well as demographic factors (age, gender).

In the classification of artificial intelligence, CVAE is considered a type of probabilistic generative deep learning model, a category that also includes generative adversarial networks, diffusion models, and language models. The way that we use CVAE, however, is not probabilistic because the conditional input to the variational autoencoder is not random, but is determined by patient characteristics such as vascular pattern, RPE elevation map, axial length, and demographics. Thus, the baseline NFL profile predicted by our model is determined by the characteristics of the eye. Since we want to use the model to predict the baseline NFL profile that would have existed without disease damage, it is important that the model input is not affected by glaucoma or other diseases. This is an

issue with the vascular pattern because glaucoma is known to attenuate retinal blood vessels.[46] Thus, we inserted a step in the vascular pattern map generation to normalize the number of vessel pixels and prevent disease from affecting the overall vessel caliber.

We developed 3 deep learning models based on CVAE. The BASE model was only based on vascular patterns and demographics. The other two generative deep learning models also incorporated information on the transverse optical magnification based either on actual measurements of AL and SE (MAG), or an rCNN that estimated AL and SE using OCT-derived vascular pattern map and RPE elevation map (REG). We found that the vascular pattern helped to align the NFLT peaks of the individualized baseline to test eyes. We also found that individualized baseline models that incorporated actual or estimated magnification information significantly outperformed the population average in terms of the prediction error and reduced the false positive glaucoma diagnosis rate in the myopic eyes. The BASE CVAE did not perform as well as MAG and REG, demonstrating that accounting for magnification-associated NFLT variation was still essential to the performance improvement achieved by our deep learning approach.

Given similar performance, the REG model may be preferable to MAG because it does not require additional AL and SE measurements. We found the two models to have similar prediction errors, but MAG was more effective in reducing the false-positive diagnosis rate in myopic eyes. The prediction error of the MAG model was smaller than that of the REG model in the validation with the CEI dataset. So, the REG model may need further improvement in generalizability. We believe that improvement may be possible by using wider maps of vascular pattern and RPE, as other investigators have found that wider-field disc photographs provided more accurate estimates of AL.[27, 36, 37]

Besides CVAE, other methods can also account for individual variation and reduce prediction error. MLR was effective in reducing prediction error for overall and some quadrant NFLT,[19, 47-49] but not the NFLT profile. The ability of CVAE to reduce prediction error for NFLT profile in regions most susceptible to glaucoma damage (superior and inferior arcuate nerve fiber bundles) may be useful in improving the detection of focal glaucoma damage. The generative AI model may be better in predicting the NFLT profile because the location and bifurcation pattern of the NFL bundles may be correlated with the vascular pattern that serves as input to the CVAE. Other investigators have also used the retinal vascular pattern as input to machine learning algorithms to improve NFLT prediction. [13, 15, 16, 50, 51] A potential advantage of our CVAE approach is that it provides highly individualized NFLT profile prediction. However, further studies are needed to compare the performance of the various approaches.

The results we presented showed that magnification-related information (AL, SE) and vascular pattern each significantly improved the accuracy of the individualized baseline reference generation. Either AL or SE alone also produced significant improvement (results not shown), but the combination was synergistic, and both clinical parameters are readily available. Therefore, we presented results for models using both AL and SE. While we did not present the individual evaluation of the importance of the other model inputs – age, sex, race, disc size, and signal strength – we found that each of them improved the performance of the models to small degrees. The effect of these predictive factors has already been shown in previously published studies.[6, 15, 19, 33, 47, 52-57]

There are several limitations to this study. First, most eyes in the Hong Kong dataset were East Asian as the dataset was obtained from Hong Kong. Literature showed that East Asians had significantly

or marginally thicker NFL than whites and blacks.[41-45] We have tried a simple proportional adjustment for race as a post-processing remedy, which works with reduced performance. It is possible that the local adjustment is different from the overall adjustment. Therefore, a better model might be achieved based on multi-racial training data and using race as a condition. The second limitation is that the model was trained with a single OCT system - the Avanti. Therefore, retraining would be needed to apply this approach to other OCT systems. The third limitation of our study is that the diagnostic sensitivity has not been tested on a group of glaucoma patients. As a more specific normative reference, we believe that the individualized baseline will improve the accuracy of NFL focal loss analysis. Our next step will be to develop an algorithm to detect focal NFL loss and assess its performance in glaucoma diagnosis. A fourth limitation is that deviation from normal reference does not necessarily indicate the presence of glaucoma – it could be due to other ocular diseases. Therefore, our individualized baseline would also need to be assessed in patients with other ocular comorbidities.

A potential pitfall of our approach is that eye diseases could affect the retinal vascular pattern and thereby the generation of the individualized NFLT baseline reference. Both glaucoma and diabetic retinopathy are known to cause attenuation of retinal vascular caliber, which may cause the AI model to generate attenuated NFLT and reduce our ability to detect NFLT loss. To make our model more disease invariant, we normalized the vessel size to keep a fixed ratio of vascular to nonvascular pixels in the vascular pattern profiles. The effectiveness of this approach will be tested in future studies on glaucoma diagnostic accuracy.

A similar pitfall is that glaucoma could affect the ILM elevation map, leading to errors in the estimation of magnification-related factors AL and SE. For that reason, we used the RPE elevation map, which would not be affected by glaucomatous thinning of NFLT, to estimate AL and SE in the MAG model.

We have demonstrated that the generative deep learning approach can generate individualized NFLT profiles, sectors, and overall values that reduce prediction error relative to simple population averages. This approach can be extended to other OCT metrics and OCT angiography metrics, such as macular ganglion cell complex thickness, NFL plexus capillary density, or cup-disc ratio.

5 Conclusions

We developed a generative deep learning AI model that can provide an individualized NFLT baseline using vascular patterns from OCT only. Compared to models based on multiple regression, the individualized baseline performed equally in reducing the population variance of global NFLT in healthy eyes or false positive rate in detected NFLT abnormality in myopia, but performed better in reducing the variance locally. The approach to constructing the individualized baseline could be extended to other OCT and OCT angiography metrics.

6 Statement:

During the preparation of this work, the author(s) used Grammarly to correct the grammar. After using this tool/service, the author(s) reviewed and edited the content as needed and take full responsibility for the content of the publication.

484

7 References

1. Quigley HA, Green WR. The histology of human glaucoma cupping and optic nerve damage: clinicopathologic correlation in 21 eyes. *Ophthalmology* 1979;86:1803-1830.
2. Medeiros FA, Alencar LM, Zangwill LM, Sample PA, Weinreb RN. The Relationship between intraocular pressure and progressive retinal nerve fiber layer loss in glaucoma. *Ophthalmology* 2009;116:1125-1133 e1121-1123.
3. Xu G, Weinreb RN, Leung CKS. Retinal nerve fiber layer progression in glaucoma: a comparison between retinal nerve fiber layer thickness and retardance. *Ophthalmology* 2013;120:2493-2500.
4. Schuman JS, Hee MR, Puliafito CA, et al. Quantification of nerve fiber layer thickness in normal and glaucomatous eyes using optical coherence tomography. *Arch Ophthalmol* 1995;113:586-596.
5. Ophthalmology AAo. 2019 AAO IRIS Registry database results in the David E. I. Pyott Glaucoma Education Center on AAO website. https://www.aao.org/education/interactive-tool/glaucoma-outcomes-iris-registry: David E.I. Pyott Glaucoma Education Center; 2019.
6. Kim MJ, Lee EJ, Kim TW. Peripapillary retinal nerve fibre layer thickness profile in subjects with myopia measured using the Stratus optical coherence tomography. *Br J Ophthalmol* 2010;94:115-120.
7. Wang G, Qiu KL, Lu XH, et al. The effect of myopia on retinal nerve fibre layer measurement: a comparative study of spectral-domain optical coherence tomography and scanning laser polarimetry. *Br J Ophthalmol* 2011;95:255-260.
8. Huang D, Chopra V, Lu AT, et al. Does optic nerve head size variation affect circumpapillary retinal nerve fiber layer thickness measurement by optical coherence tomography? *Invest Ophthalmol Vis Sci* 2012;53:4990-4997.
9. Qu D, Lin Y, Jiang H, et al. Retinal nerve fiber layer (RNFL) integrity and its relations to retinal microvasculature and microcirculation in myopic eyes. *Eye Vis (Lond)* 2018;5:25.
10. Seo S, Lee CE, Jeong JH, Park KH, Kim DM, Jeoung JW. Ganglion cell-inner plexiform layer and retinal nerve fiber layer thickness according to myopia and optic disc area: a quantitative and three-dimensional analysis. *BMC Ophthalmol* 2017;17:22.
11. Silverman AL, Hammel N, Khachatryan N, et al. Diagnostic Accuracy of the Spectralis and Cirrus Reference Databases in Differentiating between Healthy and Early Glaucoma Eyes. *Ophthalmology* 2016;123:408-414.
12. Chong GT, Lee RK. Glaucoma versus red disease: imaging and glaucoma diagnosis. *Curr Opin Ophthalmol* 2012;23:79-88.
13. Hood DC, Fortune B, Arthur SN, et al. Blood vessel contributions to retinal nerve fiber layer thickness profiles measured with optical coherence tomography. *J Glaucoma* 2008;17:519-528.
14. Yamashita T, Asaoka R, Kii Y, Terasaki H, Murata H, Sakamoto T. Structural parameters associated with location of peaks of peripapillary retinal nerve fiber layer thickness in young healthy eyes. *PLoS One* 2017;12:e0177247.
15. Mwanza JC, Lee G, Budenz DL. Effect of Adjusting Retinal Nerve Fiber Layer Profile to Fovea-Disc Angle Axis on the Thickness and Glaucoma Diagnostic Performance. *Am J Ophthalmol* 2016;161:12-21 e11-12.
16. Fujino Y, Yamashita T, Murata H, Asaoka R. Adjusting Circumpapillary Retinal Nerve Fiber Layer Profile Using Retinal Artery Position Improves the Structure-Function Relationship in Glaucoma. *Invest Ophthalmol Vis Sci* 2016;57:3152-3158.
17. Pereira I, Weber S, Holzer S, Fischer G, Vass C, Resch H. Compensation for retinal vessel density reduces the variation of circumpapillary RNFL in healthy subjects. *PLoS One* 2015;10:e0120378.
18. Resch H, Brela B, Resch-Wolfslehner C, Vass C. Position of retinal blood vessels correlates with retinal nerve fibre layer thickness profiles as measured with GDx VCC and ECC. *Br J Ophthalmol* 2011;95:680-684.

19. Liu K, Tan O, You QS, et al. Regression-Based Strategies to Reduce Refractive Error-Associated Glaucoma Diagnostic Bias When Using OCT and OCT Angiography. *Transl Vis Sci Technol* 2022;11:8.
20. Zhao Q, Adeli E, Honnorat N, Leng T, Pohl KM. Variational AutoEncoder For Regression: Application to Brain Aging Analysis. *Med Image Comput Comput Assist Interv* 2019;11765:823-831.
21. Sohn K, Lee H, Yan X. Learning Structured Output Representation using Deep Conditional Generative Models. *NIPS*; 2015.
22. Kingma DP, Rezende DJ, Mohamed S, Welling M. Semi-supervised learning with deep generative models. *Proceedings of the 27th International Conference on Neural Information Processing Systems - Volume 2.* Montreal, Canada: MIT Press; 2014:3581–3589.
23. Kingma DP, Welling M. Auto-Encoding Variational Bayes. 2013:arXiv:1312.6114.
24. Lee YJ, Sun S, Kim YK. Predicting demographic characteristics from anterior segment OCT images with deep learning: A study protocol. *PLoS One* 2022;17:e0270493.
25. Chueh KM, Hsieh YT, Chen HH, Ma IH, Huang SL. Identification of Sex and Age from Macular Optical Coherence Tomography and Feature Analysis Using Deep Learning. *Am J Ophthalmol* 2022;235:221-228.
26. Munk MR, Kurmann T, Marquez-Neila P, Zinkernagel MS, Wolf S, Sznitman R. Assessment of patient specific information in the wild on fundus photography and optical coherence tomography. *Sci Rep* 2021;11:8621.
27. Dong L, Hu XY, Yan YN, et al. Deep Learning-Based Estimation of Axial Length and Subfoveal Choroidal Thickness From Color Fundus Photographs. *Front Cell Dev Biol* 2021;9:653692.
28. Betzler BK, Yang HHS, Thakur S, et al. Gender Prediction for a Multiethnic Population via Deep Learning Across Different Retinal Fundus Photograph Fields: Retrospective Cross-sectional Study. *JMIR Med Inform* 2021;9:e25165.
29. Babu GS, Zhao P, Li X. Deep Convolutional Neural Network Based Regression Approach for Estimation of Remaining Useful Life. *International Conference on Database Systems for Advanced Applications*; 2016.
30. Leung GM, Ni MY, Wong PT, et al. Cohort Profile: FAMILY Cohort. *Int J Epidemiol* 2017;46:e1.
31. You QS, Choy BKN, Chan JCH, et al. Prevalence and Causes of Visual Impairment and Blindness among Adult Chinese in Hong Kong - The Hong Kong Eye Study. *Ophthalmic Epidemiol* 2020;27:354-363.
32. Liu L, Tan O, Ing E, et al. Sectorwise Visual Field Simulation Using Optical Coherence Tomographic Angiography Nerve Fiber Layer Plexus Measurements in Glaucoma. *Am J Ophthalmol* 2020;212:57-68.
33. Zhang X, Iverson SM, Tan O, Huang D. Effect of Signal Intensity on Measurement of Ganglion Cell Complex and Retinal Nerve Fiber Layer Scans in Fourier-Domain Optical Coherence Tomography. *Transl Vis Sci Technol* 2015;4:7.
34. Li C, Huang R, Ding Z, Gatenby JC, Metaxas DN, Gore JC. A level set method for image segmentation in the presence of intensity inhomogeneities with application to MRI. *IEEE Trans Image Process* 2011;20:2007-2016.
35. Singh A, Ogunfunmi T. An Overview of Variational Autoencoders for Source Separation, Finance, and Bio-Signal Applications. *Entropy (Basel)* 2021;24.
36. Oh R, Lee EK, Bae K, Park UC, Yu HG, Yoon CK. Deep Learning-based Prediction of Axial Length Using Ultra-widefield Fundus Photography. *Korean J Ophthalmol* 2023;37:95-104.
37. Wang Y, Wei R, Yang D, et al. Development and validation of a deep learning model to predict axial length from ultra-wide field images. *Eye (Lond)* 2023.
38. Tan O, Liu L, Zhang X, Morrison JC, Huang D. Glaucoma Increases Retinal Surface Contour Variability as Measured by Optical Coherence Tomography. *Invest Ophthalmol Vis Sci* 2016;57:OCT438-443.
39. Huang L. *Normalization Techniques in Deep Learning*: Springer International Publishing; 2022.

40. Ying GS, Maguire MG, Glynn R, Rosner B. Tutorial on Biostatistics: Statistical Analysis for Correlated Binary Eye Data. *Ophthalmic Epidemiol* 2018;25:1-12.
41. Tariq YM, Samarawickrama C, Pai A, Burlutsky G, Mitchell P. Impact of ethnicity on the correlation of retinal parameters with axial length. *Invest Ophthalmol Vis Sci* 2010;51:4977-4982.
42. Tariq YM, Li H, Burlutsky G, Mitchell P. Retinal nerve fiber layer and optic disc measurements by spectral domain OCT: normative values and associations in young adults. *Eye (Lond)* 2012;26:1563-1570.
43. Chansangpetch S, Huang G, Coh P, et al. Differences in Optic Nerve Head, Retinal Nerve Fiber Layer, and Ganglion Cell Complex Parameters Between Caucasian and Chinese Subjects. *J Glaucoma* 2018;27:350-356.
44. Ho H, Tham YC, Chee ML, et al. Retinal Nerve Fiber Layer Thickness in a Multiethnic Normal Asian Population: The Singapore Epidemiology of Eye Diseases Study. *Ophthalmology* 2019;126:702-711.
45. Nousome D, McKean-Cowdin R, Richter GM, et al. Retinal Nerve Fiber Layer Thickness in Healthy Eyes of Black, Chinese, and Latino Americans: A Population-Based Multiethnic Study. *Ophthalmology* 2021;128:1005-1015.
46. Hwang JC, Konduru R, Zhang X, et al. Relationship among visual field, blood flow, and neural structure measurements in glaucoma. *Invest Ophthalmol Vis Sci* 2012;53:3020-3026.
47. Alasil T, Wang K, Keane PA, et al. Analysis of normal retinal nerve fiber layer thickness by age, sex, and race using spectral domain optical coherence tomography. *J Glaucoma* 2013;22:532-541.
48. Ctori I, Gruppetta S, Huntjens B. The effects of ocular magnification on Spectralis spectral domain optical coherence tomography scan length. *Graefes Arch Clin Exp Ophthalmol* 2015;253:733-738.
49. Chua J, Schwarzhans F, Wong D, et al. Multivariate Normative Comparison, a Novel Method for Improved Use of Retinal Nerve Fiber Layer Thickness to Detect Early Glaucoma. *Ophthalmol Glaucoma* 2022;5:359-368.
50. Meyer SA, Durbin MK, Stetson PF, Amirbekian B. RNFL Measurement Analysis. In: https://www.uspto.gov (ed). US: Carl Zeiss Meditec Inc; 2007.
51. Hood DC, La Bruna S, Tsamis E, et al. Detecting glaucoma with only OCT: Implications for the clinic, research, screening, and AI development. *Prog Retin Eye Res* 2022;90:101052.
52. Leung CK, Yu M, Weinreb RN, et al. Retinal nerve fiber layer imaging with spectral-domain optical coherence tomography: a prospective analysis of age-related loss. *Ophthalmology* 2012;119:731-737.
53. Girkin CA, McGwin G, Jr., Sinai MJ, et al. Variation in optic nerve and macular structure with age and race with spectral-domain optical coherence tomography. *Ophthalmology* 2011;118:2403-2408.
54. Sung KR, Wollstein G, Bilonick RA, et al. Effects of age on optical coherence tomography measurements of healthy retinal nerve fiber layer, macula, and optic nerve head. *Ophthalmology* 2009;116:1119-1124.
55. Saito H, Tomidokoro A, Tomita G, Araie M, Wakakura M. Optic disc and peripapillary morphology in unilateral nonarteritic anterior ischemic optic neuropathy and age- and refraction-matched normals. *Ophthalmology* 2008;115:1585-1590.
56. Parikh RS, Parikh SR, Sekhar GC, Prabakaran S, Babu JG, Thomas R. Normal age-related decay of retinal nerve fiber layer thickness. *Ophthalmology* 2007;114:921-926.
57. Leung CK, Mohamed S, Leung KS, et al. Retinal nerve fiber layer measurements in myopia: An optical coherence tomography study. *Invest Ophthalmol Vis Sci* 2006;47:5171-5176.

8 Figure Legends

Figure 1 The nerve fiber layer (NFL) thickness map and vascular pattern; (A) ONH scan consists of circular scans (D=1.3~4.9mm) covering the peripapillary area around the optic disc; (B) OCT B-scan with NFL boundaries (solid lines) and vessel shadow detected (blue dots); (C) NFLT map and main vessel location map obtained from vessel shadow (red solid lines), the center black area masked the optic disc; (D) RNFLT profile (blue line) and vascular pattern (red dots) were resampled on the re-centered 3.4 mm circle (white dash line in Figure 1c). The vascular pattern was used as a binary mask.

Figure 1. Training of the Deep learning models. The RNFLT profile was used as a numeric array, and the vascular pattern profile was used as a binary array. (A) Overall structure of deep learning models in the training stage. It consists of a dual conditional variational autoencoder (CVAE) to reconstruct both the vascular pattern profile (VP) and the nerve fiber layer thickness profile (NFLT). Conditions blocks were different for the three deep models: BASE, MAG, and REG. The details of the conditions were shown separately in Figures 2 B-D. Note that the VP encoder's output was also used as a condition for the NFLT encoder and decoders. (B) Conditions of the BASE model include only age, gender, and signal strength index (SSI). (C) Conditions of the MAG model include conditions listed in the BASE model, plus disc area, measured axial length (AL), and spherical equivalent error (SE); (D) Conditions of the REG model are similar to the MAG model. However, AL and SE were predicted by a convolutional neural network for regression (rCNN). The rCNN used a retinal pigment epithelium elevation (RPE) map and vascular pattern map, and a binary mask of vessels was shown in Figure 1C. Other abbreviations: NFLT': estimated NFLT; VP': estimated VP; Z1 and Z2: latent variable $Z \sim N(\mu,\sigma)$: sampling in a latent space following a normal distribution of mean μ and standard deviation σ.

Figure 2. Generating the individualized baseline using deep learning models (A) Overall structure of deep learning models in the generating stage. It is much simpler compared to the training stage. Only the vascular pattern (VP) encoder and nerve fiber layer thickness (NFLT) decoder were used. The sampling layer is also removed to get the average NFL thickness, giving individual conditions. Therefore, the input of the NFLT decoder is the combination of Z1=0, Z2= μ2, and other conditions. Conditions blocks were different for the three deep models: BASE, MAG, and REG. The details of the conditions were shown in Figure 2. Other abbreviations: VP: vascular pattern; NFLT: nerve fiber layer thickness profile; NFLT': reconstructed NFLT; AL: AL; SE: spherical equivalent error; AL': estimated AL; SE': estimated SE; OC: other characteristics comprise age, gender, race, signal strength index and disc area; RPE map: retinal pigment epithelium elevation map normalized by its own mean; Z1 and Z2: latent variable.

Figure 4. The prediction error profile (thin lines) and significance mask ($p<0.05$ compared to the population average, thick lines below the axis). (A) estimated from the healthy eyes from the Hong Kong Family cohort; (B) estimated from healthy eyes from the Casey Eye Institute cohort. In both figure, the prediction error is based on the root-mean-square of the profile difference (true NFL profiles –predicted normal reference or individualized baseline) for five models: Average: population average without any adjustment; MLR: multiple linear regression model; BASE model: deep learning models using only demographic information; MAG: BASE model plus magnification information; REG: BASE model with magnification estimated with a regression convolutional neural network (rCNN); p-Value<0.05 were

666 used to check if there was a significant difference in prediction errors between the average and other
667 models.

668

669

Table 1. Characteristics of the Study Subjects from Two Cohorts

Variables	Hong Kong				CEI
	Hyperopia	Emmetropia	Low myopia	High myopia	
Participants (#)	92	233	299	62	75
Eyes(#)	136	401	509	106	75
Age (Years)	59.2±11.2	49.9±13.6	41.9±13.8	41.1±11.5	58.6±11.3
Female (%)	52.2	61.8	54.4	56.6	52.0
Spherical Equivalent (D)	2.0±1.5	0.1±0.5	-3.1±1.4	-7.8±1.6	-1.8± 3.5
Axial length (mm)	23.3±1.2	23.6±1.0	25.1±0.9	26.6±1.0	24.3± 1.5
Disc Area (mm^2)	2.2±0.4	2.2±0.4	1.9±0.4	1.7±0.4	1.9± 0.3
Average Nerve fiber layer (NFL) Thickness (µm)					
Overall	102.3±9.0	102.7±8.3	99.0±8.9	95.5±8.7	98.3± 9.5
Temporal Quadrant	78.1±9.6	78.2±9.0	79.2±9.8	82.5±10.6	74.1±10.8
Superior Quadrant	124.7±13.9	126.9±12.9	121.5±14.5	116.4±14.6	117.8±14.6
Nasal Quadrant	76.6±10.1	75.9±10.2	69.4±10.4	64.9±10.8	77.0±10.3
Inferior Quadrant	129.8±12.5	129.9±12.9	125.8±13.7	118.2±13.8	124.2±14.3

Values for continuous variables are means ± standard deviations. Disc area is not magnification adjusted. FSOCT is the second dataset; CEI=Casey Eye Institute

Table 2. Association between Nerve Fiber Layer Thickness and Predictive Factors (Hong Kong Family Cohort)

Slopes	*Group*	*Overall Average NFL*	*Quadrant Average NFL*			
			Temporal	*Superior*	*Nasal*	*Inferior*
Axial length ***(µm/mm)***	*Myopia*	*-2.65***	*0.72*	*-4.05***	*-3.22***	*-4.04***
	Hyperopia	*-1.47***	*0.41*	*-2.00***	*-2.16***	*-2.11***
Age ***(µm/Years)***		*-0.14***	*-0.12***	*-0.23***	*0.00*	*-0.20***
*Female****(µm)***		*0.89*	*2.67***	*-1.23*	*-0.69*	*2.79***
SSI ***(µm)***		*0.04*	*-0.00*	*0.10*	*0.02*	*0.02*

**p<0.01, **p<0.005, SE=Spherical equivalent refractive error . Accounting for multiple comparisons of 4 quadrant values plus the overall value, the Bonferroni correction was used to set the p-value cutoff at 0.01 for statistical significance. Gender difference is calculated by female – male.*

+ Slopes against axial length were different between myopia segment and hyperopia segment using the broken stick model, which divided the healthy eyes into two segments with break point at the spherical equivalent refractive error =0

Table 3. Prediction Error (µm) of Nerve Fiber Layer Thickness in Healthy Eyes in Two Cohorts

		Quadrant Average			
Models	**Overall**	**Temporal**	**Superior**	**Nasal**	**Inferior**
Hong Kong					
Average	8.99±0.58	9.63±0.44	14.28±1.04	11.08±0.73	13.74±0.35
MLR	8.32±0.57*	9.36±0.30	13.35±0.85+	10.31±0.84+	12.60±0.48*
BASE	8.93±0.59	8.97±0.37+	13.76±0.78	10.75±0.88	13.61±0.54
MAG	8.18±0.51*	8.99±0.25+	13.15±0.82*	9.65±0.70*	12.91±0.52+
REG	8.16±0.47*	9.04±0.33+	13.07±0.64*	9.56±0.64*	12.98±0.39+
Casey Eye Institute					
Average	9.63	10.82	14.42	10.58	14.27
MLR	8.67	10.01*	13.13	10.13	13.17
BASE	9.10+	9.89+	13.61	11.42	13.63
MAG	8.41+	9.57	12.56	9.52	13.66
REG	8.72*	9.98	13.23	10.46	13.90

MLR=model based on multiple linear regression; BASE: deep learning model trained with conditions of vascular pattern and demographic information, MAG: BASE model with extra conditions of measured axial length and spherical equivalent refractive error . REG: similar to MAG model, but the axial length and spherical equivalent refractive error were estimated by a convolutional neural network for regression.

**, p<0.0125 and +, p<0.05, comparing to the Average model*

Table 4. False Positive Rate Based on 5 Percentile Cutoff Estimated from Emmetropia Eyes (Hong Kong Family Cohort)

Eye Group	*Models*	*Overall*	*Temp*	*Sup*	*Nasal*	*Inf*
	Average	*7.6%*	*5.1%*	*10.1%*	*3.2%*	*5.7%*
	MLR	*6.3%*	*4.4%*	*10.1%*	*5.7%*	*4.4%*
Hyperopia	*BASE*	*4.4%*	*5.1%*	*7.0%*	*4.4%*	*4.4%*
	MAG	*4.4%*	*5.7%*	*8.2%*	*5.7%*	*3.8%*
	REG	*5.1%*	*3.2%*	*10.1%*	*5.7%*	*5.1%*
	Average	*13.3%*	*2.6%*	*13.9%*	*15.4%*	*10.1%*
	MLR	*8.3%**	*4.0%*	*8.7%**	*8.7%**	*6.3%**
Low Myopia	*BASE*	*13.5%+*	*3.8%*	*13.3%+*	*11.9%*+*	*10.7%+*
	MAG	*6.7%**	*4.4%*	*7.1%**	*5.7%*+*	*4.6%**
	REG	*9.1%**	*5.1%**	*7.7%**	*6.1%**	*6.1%**
	Average	*27.1%*	*3.1%*	*22.9%*	*31.3%*	*25.0%*
	MLR	*5.2%**	*7.3%*	*10.4%**	*6.3%**	*8.3%**
High Myopia	*BASE*	*20.8%+*	*8.3%*	*20.8%+*	*16.7%*+*	*18.8%*
	MAG	*6.3%**	*7.3%*	*4.2%**	*7.3%**	*6.3%**
	REG	*9.4%**	*4.2%**	*11.5%**	*5.2%**	*12.5%**

MLR=model based on multiple linear regression; BASE: deep learning model trained with conditions of vascular pattern and demographic information, MAG: BASE model with extra conditions of measured axial length and spherical equivalent refractive error . REG: similar to MAG model, but the axial length and spherical equivalent refractive error were estimated by a convolutional neural network for regression.

** p-value<0.0125 comparing to average, + p-value<0.0125 comparing to MLR method*

Table 5. Difference between the Normal Reference Mean and 5 percentile Cut-Point(Hong Kong Family Cohort)

		Quadrant Average			
Models	*Overall*	*Temporal*	*Superior*	*Nasal*	*Inferior*
Average	*14.9±0.7*	*14.5±1.2*	*23.4±1.8*	*18.9±1.7*	*22.7±0.9*
MLR	*13.7±0.9*	*14.7±1.4*	*21.8±2.3*	*17.0±2.2**	*20.5±1.0+*
BASE	*14.2±1.0*	*13.9±1.3*	*21.0±1.0+*	*17.3±1.6**	*22.7±0.9*
MAG	*13.3±0.6+*	*13.7±0.7*	*21.3±0.7*	*15.6±1.5**	*20.4±1.0**
REG	*13.0±0.6**	*14.1±1.7*	*21.0±0.6*	*15.2±0.8**	*20.8±1.6*

MLR=model based on multiple linear regression; BASE: deep learning model trained with conditions of vascular pattern and demographic information, MAG: BASE model with extra conditions of measured axial length and spherical equivalent refractive error . REG: similar to MAG model, but the axial length and spherical equivalent refractive error were estimated by a convolutional neural network for regression.

*P<0.0125, +p<0.05 compared to the population average model

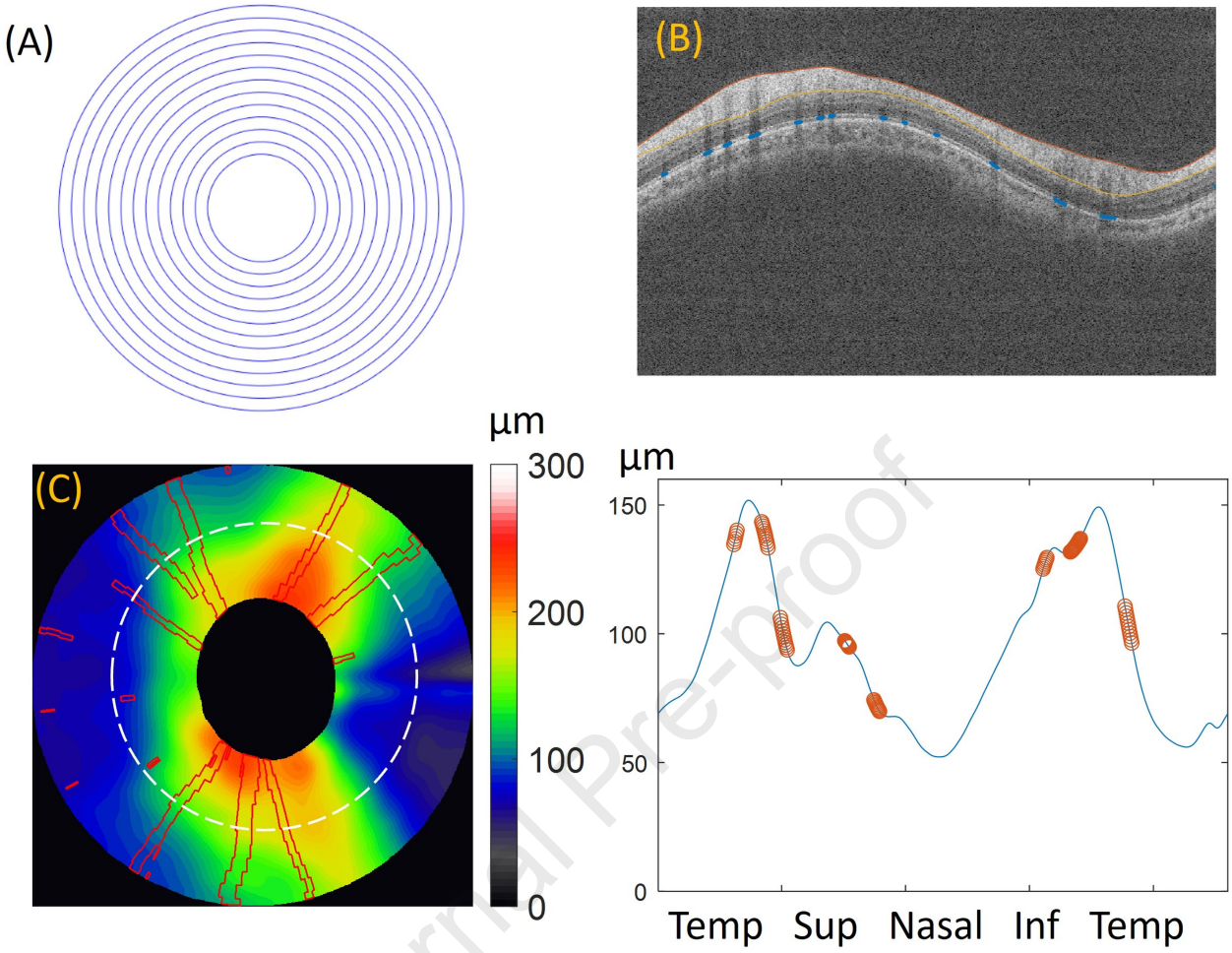

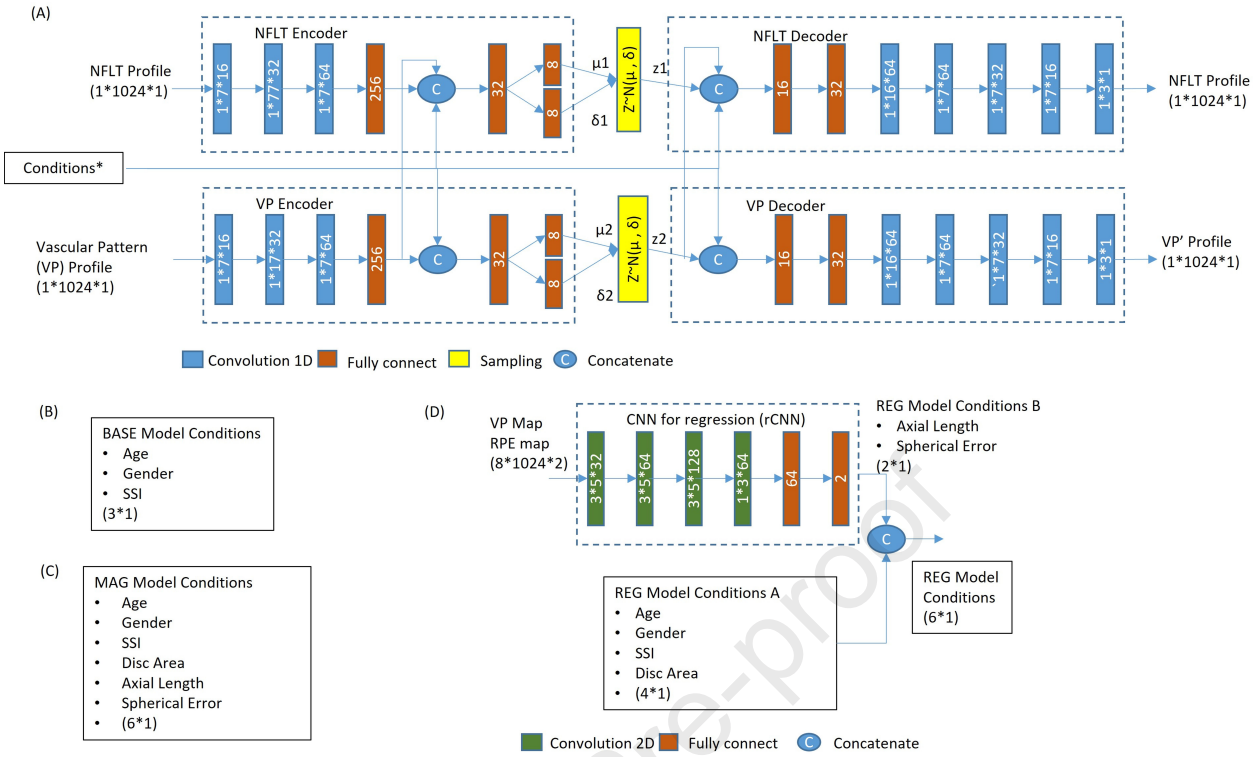

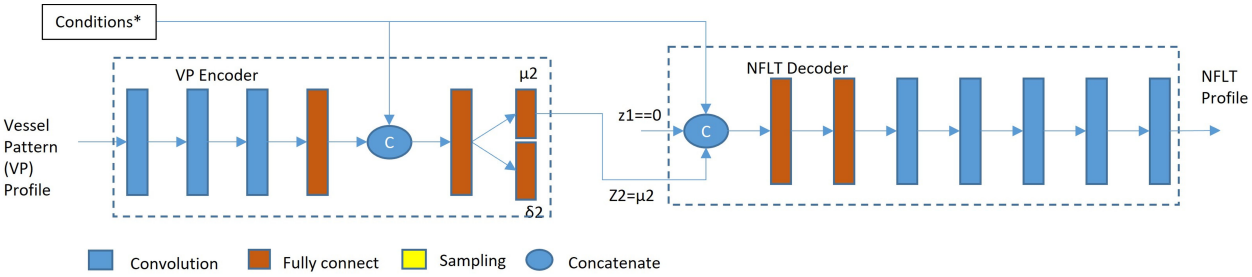

(A)

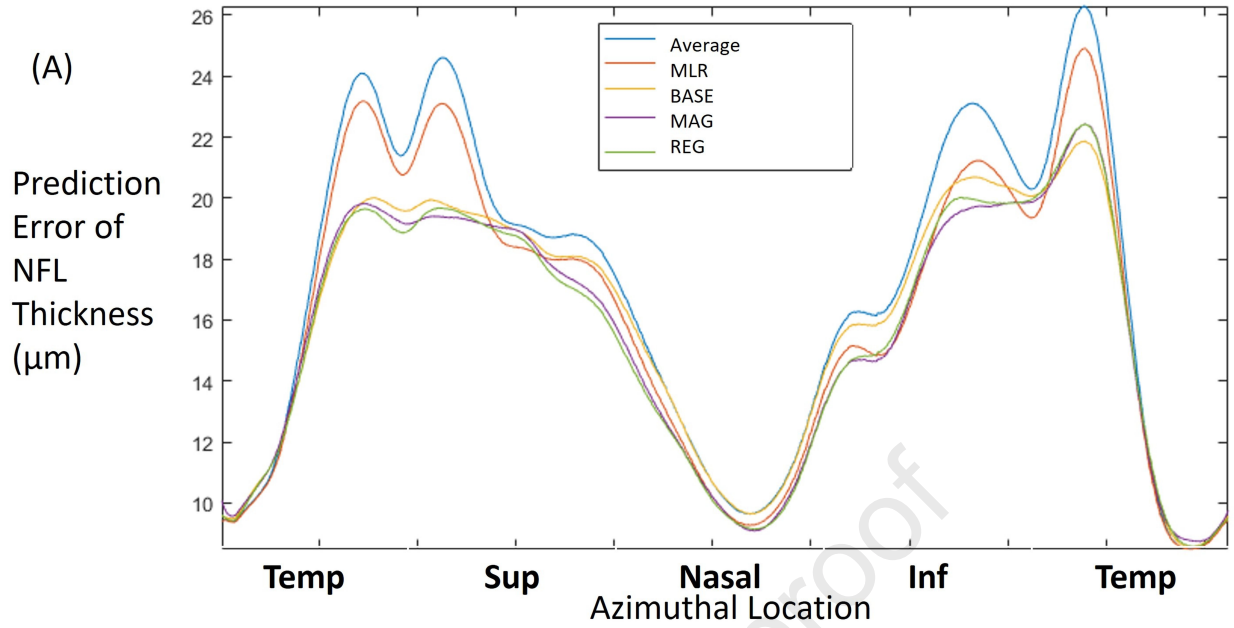

P<0.05 compared to Average

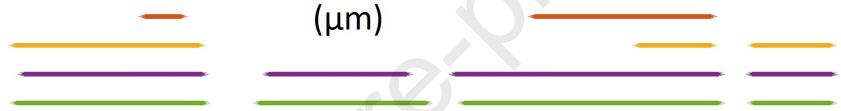

(B)

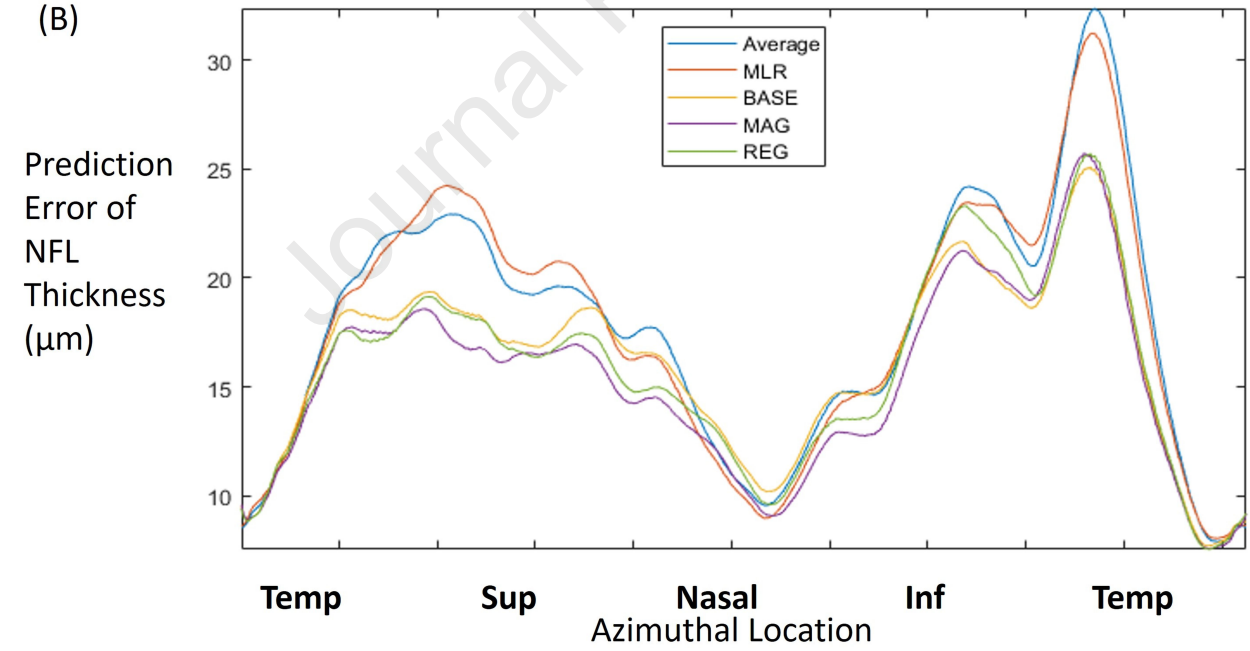

Generative deep learning model provides individualized baseline, a customized normal reference based on demographic information and individual vascular pattern, for nerve fiber layer thickness to reduce the bias in glaucoma abnormal test